Japanese Journal of Applied Physics

REGULAR PAPER

Ion-gel-based light-emitting devices using transition metal dichalcogenides and hexagonal boron nitride heterostructures

Japanese Journal of Applied Physics **62**, SC1026 (2023) **REGULAR PAPER**
https://doi.org/**10.35848/1347-4065/acaeb2**

Ion-gel-based light-emitting devices using transition metal dichalcogenides and hexagonal boron nitride heterostructures

Hao Ou[1], Koshi Oi[1], Rei Usami[1], Takahiko Endo[2], Yasumitsu Miyata[2], Jiang Pu[1*], and Taishi Takenobu[1*]

[1]*Department of Applied Physics, Nagoya University, Nagoya 464-8603, Japan*
[2]*Department of Physics, Tokyo Metropolitan University, Tokyo 192-0397, Japan*

[*]E-mail: jiang.pu@nagoya-u.jp; takenobu@nagoya-u.jp

Received October 21, 2022; revised December 16, 2022; accepted December 26, 2022; published online January 23, 2023

Fabrication of high-performance optoelectronic devices is an important aspect of the application research of transition metal dichalcogenides (TMDCs). In this study, heterostructures of TMDCs and hexagonal boron nitrides (hBN) were successfully fabricated into light-emitting devices. Monolayer and artificially stacked homobilayer WS_2 were prepared on hBN, respectively. They were then deposited with electrodes and covered by the ion gels to function as light-emitting devices. Both devices showed clear electroluminescence (EL) with voltages of ~3 V. In monolayer device, a symmetric EL peak was observed with suppressed inhomogeneity. The bilayer device showed spectra that agreed with the natural bilayer samples. These results indicate the enhancement of the optical performance of TMDCs and the heterostructure could expand the potential of TMDC-based light-emitting devices.

1. Introduction

Atomic-layer transition metal dichalcogenides (TMDCs) possess attractive optical, optoelectronic, and quantum properties, owing to their two-dimensional nature and diverse bandgaps.[1)] There are numerous reports on TMDC-based optoelectronic device applications, such as light-emitting diodes,[2,3)] photodetectors,[3)] and lasers.[4)] Moreover, the unique spin-valley coupling effect enables the TMDCs to be fabricated into information transmitters by means of chiral light emission.[5,6)] For example, it has been known that circularly polarized light pumping leads to a selective population of one valley of monolayer MoS_2, resulting in robust circularly polarized photoluminescence (PL).[7,8)] Further, it has been demonstrated that the monolayer WS_2 light-emitting devices produced circularly polarized electroluminescence (EL).[9,10)] More recently, the homo- or heterobilayers of TMDCs invoked exotic optical properties, such as the existence of moiré exciton, which controls the circularly polarized light emission because of the distinct optical selection rule of the interlayer hopping.[11–14)] These significant properties of atomic-layer TMDCs guarantee the potential of utilizing them as functional optoelectronic devices.

To realize high-performance TMDC-based light-emitting devices, photodiodes, and other optical devices, one key point is to modulate the excitonic coupling between the TMDC active materials and substrates. In most cases, TMDC thin flakes are grown or transferred onto the Si/SiO_2 substrate followed by device fabrication and characterization. The device performance is typically affected by the roughness, charged impurities, and unintentional doping originating from the SiO_2 surface.[15)] On the other hand, there have been reports on the possible modulating effect on carrier behavior when encapsulating TMDCs with hexagonal boron nitride (hBN).[16–20)] The PL intensity of intralayer excitons can significantly increase and their spectral resolution can be enhanced, such as the clear separation between exciton and trion peaks, because of the reduced local inhomogeneities and nonradiative recombination by hBN encapsulation.[19,20)] Meanwhile, hBN is often used as a supporting layer in the "dry-transfer" method for picking-up and transferring monolayers or fabricating bilayer/multilayer heterostructures.[21–23)] The device performance should be well improved if light-emitting devices based on TMDC/hBN heterostructures can directly be fabricated. Although there have been few studies on the EL of this material system,[24,25)] the detailed study and characterization of TMDC/hBN light-emitting devices are still limited. The technical issue in terms of constructing a light-emitting device directly on TMDC/hBN heterostructures can be a possible reason, that is, when using the current dry-transfer method, the TMDC is either sandwiched by hBN and Si/SiO_2 substrate or encapsulated by hBN flakes.[21)] Both structures require complicated electrode patterning, which hampers further device designs to enhance device utilities and functionalities. Therefore, a simple light-emitting device being applicable with TMDC/hBN heterostructure is required.

Recently, we developed a simple ion-gel-based light-emitting device structure utilizing ion gel as gating material, which enables a high doping level inside the TMDC,[26,27)] and EL can be generated by applying a voltage difference between two electrodes on TMDCs.[28–30)] If the ion-gel-based device structure can be applied to TMDC/hBN heterostructures, we could expect easy-to-fabricate light-emitting devices with an improvement in EL properties. In this study, we report on the fabrication of ion-gel-based light-emitting devices using the WS_2/hBN heterostructures. We proved that EL can be generated in either monolayer or homobilayer WS_2 devices on hBN, simply by applying a few volts of voltage. Spectral analysis of EL showed that with hBN substrate, the fabricated devices exhibit noticeable performances, such as the high exciton peak homogeneity. Compared to our previous report on Solid State Devices and Materials (SSDM2022),[30)] we extended the objectives of light-emitting device structure to TMDC/hBN heterostructures, showing that the structure is suitable for a versatile material choice with variable device performances. Our results provide an integrated new method for the study of optoelectronic device application of atomic-layer materials.

2. Experimental methods

To directly fabricate TMDC/hBN heterostructure light-emitting device and drive it into EL, we employed a polymer-assisted flip transfer method which was developed

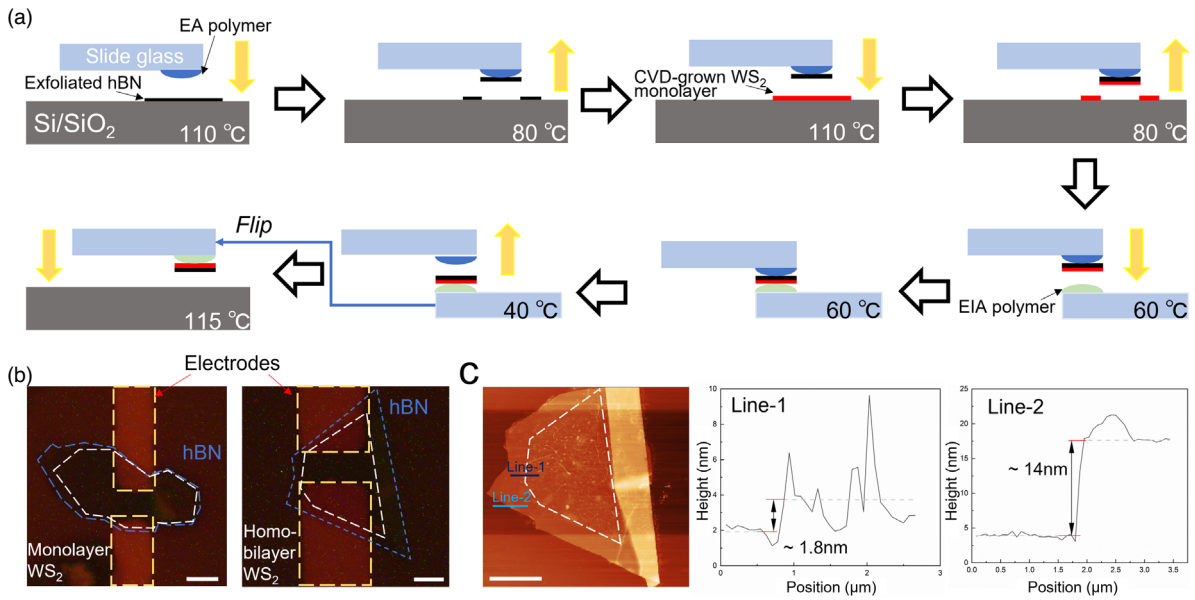

Fig. 1. (Color online) (a) Fabrication procedure of the monolayer WS_2/hBN heterostructure. An exfoliated hBN flake (thickness = 10–30 nm) is picked up by the EA polymer, then hBN is used to pick up monolayer WS_2. The obtained heterostructure is then transferred to EIA polymer by flip transfer method. The slide glass carrying EIA will be flipped to deposit the heterostructure onto Si/SiO_2 substrate. Using this method, one side of WS_2 is exposed for further processes. The transfer procedure of near 0° homobilayer WS_2/hBN heterostructure is similar to the process above, only that two monolayers are picked up sequentially by hBN flake before flip transfer. (b) Optical images of fabricated monolayer (left) and homobilayer (right) WS_2 light-emitting devices on hBN. Ion gel was already spin-coated on the surfaces of heterostructure and electrodes. (c) Left: AFM image of the obtained homobilayer WS_2 and hBN heterostructure. Line roughness profiles along lines 1 and 2 are shown in the right panel. All scale bars in (b) and (c) are 5 μm.

recently.[31] We used CVD-grown monolayer WS_2 samples to fabricate heterostructures. Compared with exfoliated monolayers, synthesized WS_2 are triangles with several tens to more than one hundred micrometers,[32,33] making it possible to fabricate large-area devices in future 2D material-based electronics. As shown in Fig. 1(a) of the fabrication procedure of monolayer TMDC/hBN heterostructure, CVD-grown monolayer WS_2 was first picked up by hBN thin flake (exfoliated from bulk hBN bought from 2D Semiconductors) at 80 °C using the polymer-assisted dry-transfer method.[34] We used Elvacite polymer (E2552C. Mitsubishi Chemical) in anisole solvent (weight ratio = 1:1.5, *abbr.* EA). To conduct dry-transfer, one drop of viscous solution was taken onto a slide glass using a toothpick. The slide glass was then placed on a hotplate at 180 °C for 1 h to evaporate solvent and leave only polymer. At this stage, hBN was above the monolayer, and if we directly transferred the heterostructure onto the Si/SiO_2 substrate, TMDC would be encapsulated between hBN and substrate, which could have resulted in difficulty in constructing light-emitting device directly on TMDCs. Therefore, to fabricate a light-emitting device more easily, we flipped the contact between heterostructure and polymer such that one side of the TMDC will be exposed when transferred onto the substrate.[31] It is worth noting that we conducted the flip transfer utilizing a new polymer by mixing Elvacite with an ionic liquid in an anisole solvent (weight ratio Elvacite: ionic liquid: anisole = 1:0.4:1.5, *abbr.* EIA). The ionic liquid used here was 1-Ethyl-3-methylimidazolium bis(trifluoromethylsulfonyl)imide ([EMIM][TFSI]). The preparation of EIA polymer on slide glass is the same as EA polymer. Because of the viscosity difference between the two types of polymers, the heterostructure could be transferred onto EIA polymer at 40 °C with TMDC sandwiched by EIA polymer and hBN. The detailed transfer procedure and transfer stage temperature values are shown in Fig. 1(a). The heterostructure was then deposited on Si/SiO_2 substrate together with EIA polymer at 115 °C. Finally, the residing EIA polymer was removed by immersing the substrate in chloroform (1 min), acetone (30 min), and IPA (30 min). We further fabricated near 0° homobilayer WS_2/hBN heterostructures besides monolayer/hBN heterostructures. The fabrication of homobilayer WS_2 was similar to the above-mentioned procedure, except for further TMDC monolayer picking-up before flip transfer. All the fabricated heterostructure samples were annealed at 200 °C in vacuum for 8 h. The samples were then processed with electrode deposition (Ni 3 nm, Au 100 nm), patterned via photolithography. The obtained samples with electrodes are shown in Fig. 1(b). Further, we measured the AFM image of the obtained homobilayer WS_2. Left of Fig. 1(c) is the morphology image in the AFM measurement, and the linear roughness profiles along two lines (lines 1 and 2) are shown in the right part. It is shown from line 1 profile that the TMDC region has a thickness of approximately 1.8 nm, which is comparable to the reported value of CVD-grown WS_2.[35] The thickness of hBN was approximately 14 nm [line 2 profile in Fig. 1(c)].

We then converted the samples to a light-emitting device configuration. Ion gel, which is the mixture of ion liquid ([EMIM][TFSI]) and triblock co-polymer (PS-PMMA-PS, M_{PS} = 5.0 kg mol^{-1}, M_{PMMA} = 13.0 kg mol^{-1}, and M_w = 23.0 kg mol^{-1}) was dissolved in a solvent (ethyl propionate). Solution weight ratio was maintained as [EMIM][TFSI]: PS-PMMA-PS: ethyl propionate = 0.7:9.3:90. The obtained ion gel was spin-coated onto the surfaces of electrodes and TMDC (rpm = 6000 for 120 s). The schematic of the ion gel-based light-emitting device is presented in Fig. 2(a).[28] When we apply voltage drop between two electrodes, the anions and cations inside the ion gel redistribute to the surfaces of

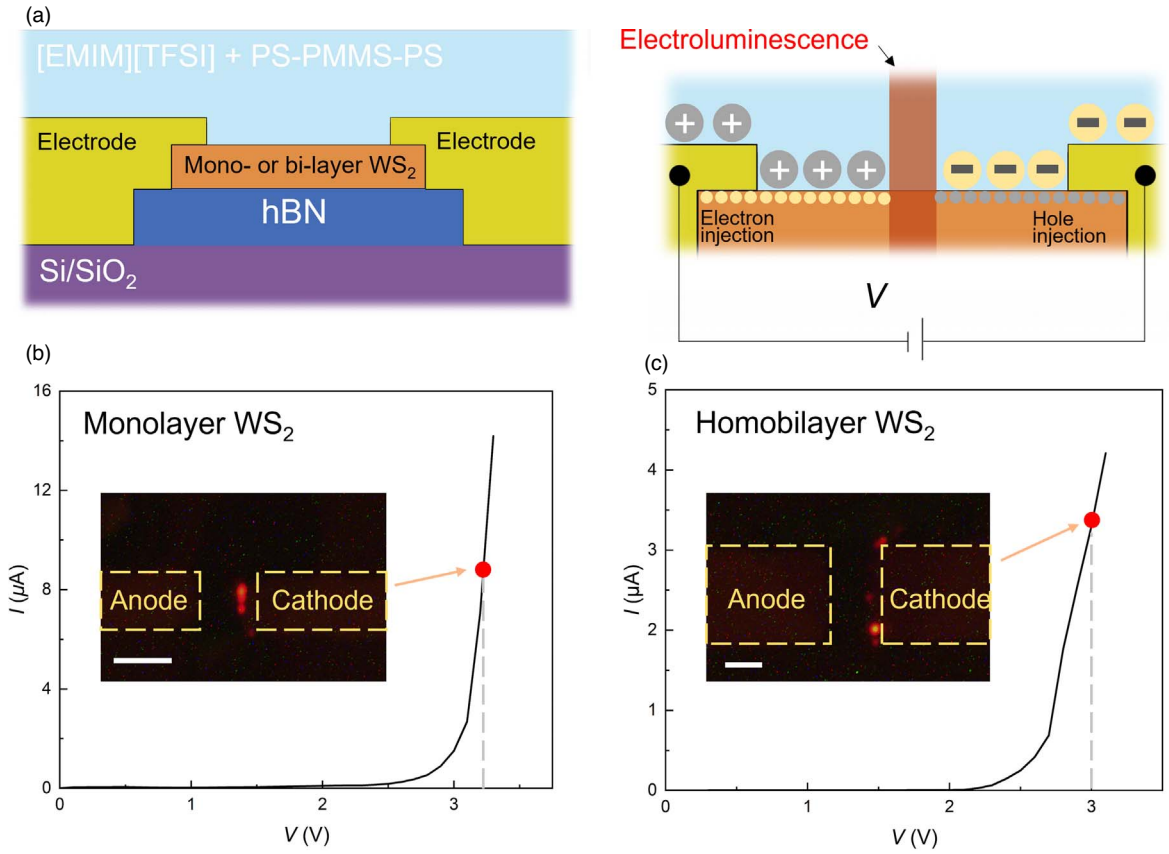

Fig. 2. (Color online) (a) Left: schematic of the light-emitting device structure. Right: working principle of the device. When applying voltage drop between two electrodes. The redistribution and accumulation of anions and cations in ion gels lead to the electron/hole injection into the TMDCs. They recombine in the channel region to generate EL. (b) *I–V* curve of monolayer WS_2/hBN heterostructure light-emitting device, with EL image at 3.2 V (inset). (c) *I–V* curve of homobilayer WS_2/hBN heterostructure light-emitting device, with EL image at 3.0 V (inset). Scale bars in (b) and (c) are both 5 μm.

electrodes and TMDCs, in response to the electric force, and the number of accumulated ions increases with increasing voltage. Consequently, ambipolar transport appears in the TMDC, with electrons and holes simultaneously injected and recombined in the channel region. Further on increasing the applied voltage, *p–i–n* junction is formed to generate EL.

3. Results and discussion

We successfully observed room-temperature EL for both devices made with monolayer and homobilayer WS_2/hBN heterostructures, as shown in Figs. 2(b) and 2(c). The *I–V* curves were collected using a semiconductor parameter analyzer (Agilent Technologies, Inc. E5270). Note that with the large effective capacitance of electric double layer (EDL) formed at the interface between ion gels and TMDCs, which offers a large electric field and strong gating effect to the TMDCs, the voltage required for large carrier injection and generation of EL was lower than 3 V. Consequently, *p–i–n* junction was formed in the channel region of the device under a relatively low driving voltage. From insets of Figs. 2(b) and 2(c), it can be noticed that when the magnitude of the injected current was of μA level, EL was captured by a CCD camera (SHODENSHA). To avoid possible electrochemical reactions, we collected EL images of devices at ~3.0 V.

Figures 3(a) and 3(b) show the EL spectra of fabricated light-emitting devices collected by a spectrometer (Hamamatsu Photonics K. K.). For comparison, we also present the PL spectra of monolayer WS_2 and homobilayer WS_2/hBN. The wavelength of the laser is 532 nm (JASCO NRS-5100) and exciting power of 130 μW was adopted, as shown in Figs. 3(a) and 3(b). For both PL and EL spectra of the monolayer WS_2/hBN device, a peak between 1.9 and 2.0 eV was observed corresponding to the excitonic peak of monolayer WS_2. Note that the peak position and full-width half-maximum of the EL spectrum were slightly different from those of PL, possibly because of the doping-induced electric-optical interaction in the EL process, in which quantum-confined Stark effect and doping-induced band structure modulation resulted in the redshift and broadening of exciton peak.[36] The significant redshift of EL peak energy from that of PL indicates that in the EL, the carrier recombination could possibly occur in p- and/or n-doped regions and the EL property is affected by carrier doping. The EL peak is quite symmetric owing to suppressed inhomogeneous broadening, which can be attributed to the hBN substrate, as it frees the TMDC from the influence of SiO_2 surface roughness and/or charge transfer-induced doping effect. The above results show that by using hBN substrate, it was possible to probe the excitonic property modulation in EL of TMDC. However, the difference between PL and EL peaks indicates that to reveal EL with the same energy and being as comparably sharp as PL in the monolayer device, further optimization of device fabrication and working condition is required.

To prove that a good contact between TMDC and hBN substrate is built after the flip transfer, and to show that the proposed device structure is also applicable for multi-

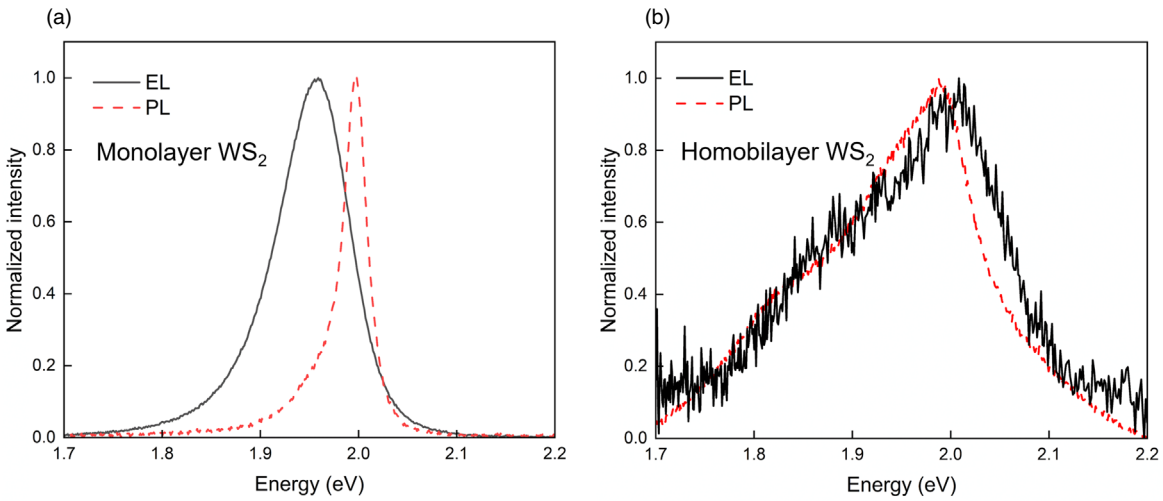

Fig. 3. (Color online) (a) EL (black solid line) and PL (red dash line) spectra measured for monolayer WS_2/hBN heterostructure light-emitting device. The applied voltage for EL spectrum measurement is 3.2 V. (b) EL (black solid line) and PL (red dash line) spectra of homobilayer WS_2/hBN heterostructure light-emitting device. The applied voltage for EL spectrum measurement is 3.0 V.

stacking TMDC system, we further fabricated homobilayer WS_2/hBN heterostructure. Note that we did not directly use the natural bilayer WS_2; however, we obtained the homobilayer by stacking two individual monolayers using hBN. The twist angle was $\sim 0° \pm 1°$, considering the precision of the transfer stage. Typically, CVD-grown monolayer TMDCs have a triangle shape with edges along the zigzag direction.[37] Therefore, we could easily identify the existence of a single-crystal WS_2 monolayer. Furthermore, because the size of exfoliated hBN ($\sim 20\ \mu$m) is much smaller than that of the CVD-grown monolayer (more than 100 μm), we could pick up two monolayer flakes continuously within the same single-crystal. Because the transfer stage was not rotated during the picking-up process, the twist angle was maintained at about 0°. Clear EL was observed for homobilayer WS_2/hBN heterostructure devices, as shown in Figs. 2(c) and 3(b). Being different from the monolayer, the PL spectrum of WS_2 homobilayer has a lower peak intensity, which is similar to that of the reported natural bilayer MoS_2.[38] Therefore, the spectra collected were not as smooth as that of a monolayer device. Furthermore, the PL spectrum shows two peaks, which are energetically recognized as exciton and trion peaks, possibly owing to the enhanced trion-origin emission arising from the interlayer coupling.[39] This property was also revealed in the EL spectrum, as two-peak behaviors with identical intensities are observable. Nevertheless, clear PL and EL spectra with similar peak energies were observed, indicating that our ion-gel-based light-emitting device structure could readily drive the artificially stacked homobilayer TMDC system into EL emission with sufficient driving voltage. Interestingly, the peak energy shift of EL from PL in the homobilayer device was not as significant as that in the monolayer, possibly owing to a lower doping level in the homobilayer. One possible reason is the large contact resistance between the electrode and the sample. A large portion of the voltage drop was applied at the contact region, and the electrostatic doping on the sample was relatively low. Another possibility is the doping inside bilayer. Under the same doping level, the carrier density per layer in the bilayer was approximately halved compared with that of the monolayer, which made the bilayer device more difficult to emit high-intensity EL or exhibit significant redshift of EL peak energy. Moreover, the band renormalization effect in the bilayer could be different from that in the monolayer. The different optical performances between monolayer and homobilayer devices also showed that the transfer process is suitable for fabricating multi-stacked TMDC light-emitting devices. Together with hBN substrate, the excitons (trions) can exhibit homogeneous emission; consequently, our light-emitting device structure functions as a good platform for exploring the carrier dynamics during EL. For example, it becomes possible to investigate in detail the electrically controlled behaviors, transient transport properties, and many-body effects of intra- and inter-layer excitons (trions) in bilayer TMDC light-emitting devices.

4. Conclusions

We successfully fabricated the TMDC/hBN heterostructure light-emitting devices by combining the flip transfer method and ion-gel-based light-emitting device structure. Clear EL emission images were collected in both monolayer WS_2 and homobilayer WS_2 devices on hBN. Further analysis of EL and PL spectra verified hBN's modulating effect on the excitonic behaviors of the TMDCs. With hBN substrates, the obtained light-emitting devices can emit spectrally symmetric EL, and well identifiable exciton and trion peaks. Our results reveal the potential of utilizing hBN in high-performance optoelectronic devices and also provide an approach for studying the detailed EL properties of TMDCs. Further, the good performance exhibited in this study indicates the potential of utilizing CVD-grown samples in device applications.

Acknowledgments

H. Ou thanks M. Sakano and Y. Tanaka for the fruitful discussion. This work was financially supported by the Japan Science and Technology Agency (JST) CREST program (JPMJCR16F3 and JPMJCR17I5), the JST FOREST Program (JPMJFR213X), and KAKENHI Grant-in-Aids (JP17H01069, JP18H01832, JP19H02543, JP19K15383,

JP19K22127, JP20H02605, JP20H05664, JP20H05862, JP20H05867, JP20K05413, JP20H05189, JP21H05232, JP21H05234, JP21H05236, JP22J13784, JP22H00280, JP22H00283, JP22H00215, JP22H04957, JP22K19059, JP26102012, and JP25000003) from the Japan Society for the Promotion of Science (JSPS).

1) Q. H. Wang, K. Kalantar-Zadeh, A. Kis, J. N. Coleman, and M. S. Strano, Nat. Nanotechnol. **7**, 699 (2012).
2) J. Pu and T. Takenobu, Adv. Mater. **30**, 1707627 (2018).
3) Y.-Q. Bie et al., Nat. Nanotechnol. **12**, 1124 (2017).
4) Y. Ye, Z. J. Wong, X. Lu, X. Ni, H. Zhu, X. Chen, Y. Wang, and X. Zhang, Nat. Photonics **9**, 733 (2015).
5) D. Xiao, G.-B. Liu, W. Feng, X. Xu, and W. Yao, Phys. Rev. Lett. **108**, 196802 (2012).
6) X. Xu, W. Yao, D. Xiao, and T. F. Heinz, Nat. Phys. **10**, 343 (2014).
7) H. Zeng, J. Dai, W. Yao, D. Xiao, and X. Cui, Nat. Nanotechnol. **7**, 490 (2012).
8) K. F. Mak, K. He, J. Shan, and T. F. Heinz, Nat. Nanotechnol. **7**, 494 (2012).
9) Y. J. Zhang, T. Oka, R. Suzuki, J. T. Ye, and Y. Iwasa, Science **344**, 725 (2014).
10) J. Pu, W. Zhang, H. Matsuoka, Y. Kobayashi, Y. Takaguchi, Y. Miyata, K. Matsuda, Y. Miyauchi, and T. Takenobu, Adv. Mater. **33**, 2100601 (2021).
11) Z. Wang, Y.-H. Chiu, K. Honz, K. F. Mak, and J. Shan, Nano Lett. **18**, 137 (2018).
12) H. Yu, G.-B. Liu, J. Tang, X. Xu, and W. Yao, Sci. Adv. **3**, e1701696 (2017).
13) K. L. Seyler, P. Rivera, H. Yu, N. P. Wilson, E. L. Ray, D. G. Mandrus, J. Yan, W. Yao, and X. Xu, Nature **567**, 66 (2019).
14) K. Tran et al., Nature **567**, 71 (2019).
15) O. A. Ajayi et al., 2D Mater. **4**, 031011 (2017).
16) F. Cadiz et al., Phys. Rev. X **7**, 021026 (2017).
17) G. Wang, A. Chernikov, M. M. Glazov, T. F. Heinz, X. Marie, T. Amand, and B. Urbaszek, Rev. Mod. Phys. **90**, 021001 (2018).
18) M. Goryca et al., Nat. Commun. **10**, 4172 (2019).
19) C. R. Dean et al., Nat. Nanotechnol. **5**, 722 (2010).
20) G.-H. Lee et al., ACS Nano **9**, 7019 (2015).
21) A. Castellanos-Gomez, M. Buscema, R. Molenaar, V. Singh, L. Janssen, H. S. J. van der Zant, and G. A. Steele, 2D Mater. **1**, 011002 (2014).
22) Y. Cao et al., Nature **556**, 80 (2018).
23) K. Kinoshita, R. Moriya, M. Onodera, Y. Wakafuji, S. Masubuchi, K. Watanabe, T. Taniguchi, and T. Machida, npj 2D Mater. Appl. **3**, 1 (2019).
24) J. S. Ross et al., Nat. Nanotechnol. **9**, 268 (2014).
25) J. Wang, F. Lin, I. Verzhbitskiy, K. Watanabe, T. Taniguchi, J. Martin, and G. Eda, Nano Lett. **19**, 7470 (2019).
26) J. T. Ye, Y. J. Zhang, R. Akashi, M. S. Bahramy, R. Arita, and Y. Iwasa, Science **338**, 1193 (2012).
27) D. Costanzo, S. Jo, H. Berger, and A. F. Morpurgo, Nat. Nanotechnol. **11**, 339 (2016).
28) J. Pu, T. Fujimoto, Y. Ohasi, S. Kimura, C.-H. Chen, L.-J. Li, T. Sakanoue, and T. Takenobu, Adv. Mater. **29**, 1606918 (2017).
29) H. Ou et al., ACS Nano **15**, 12911 (2021).
30) H. Ou, J. Pu, T. Yamada, N. Wada, H. Naito, Z. Liu, T. Irisawa, K. Yanagi, Y. Miyata, and T. Takenobu, Ext. Abstr. Solid State Devices and Materials, 2022, p. 597.
31) S. Masubuchi et al., Sci. Rep. **12**, 10936 (2022).
32) J. Pu et al., Adv. Mater. **34**, 2203250 (2022).
33) N. Wada et al., Adv. Funct. Mater. **32**, 2203602 (2022).
34) S. Masubuchi, M. Morimoto, S. Morikawa, M. Onodera, Y. Asakawa, K. Watanabe, T. Taniguchi, and T. Machida, Nat. Commun. **9**, 1413 (2018).
35) D. Thakur, P. Kumar, S. M. , R. Ramadurai, and V. Balakrishnan, Surf. Interfaces **26**, 101308 (2021).
36) J. Pu, K. Matsuki, L. Chu, Y. Kobayashi, S. Sasaki, Y. Miyata, G. Eda, and T. Takenobu, ACS Nano **13**, 9218 (2019).
37) A. M. van der Zande, P. Y. Huang, D. A. Chenet, T. C. Berkelbach, Y. You, G.-H. Lee, T. F. Heinz, D. R. Reichman, D. A. Muller, and J. C. Hone, Nat. Mater. **12**, 554 (2013).
38) W. Zhao, Z. Ghorannevis, L. Chu, M. Toh, C. Kloc, P.-H. Tan, and G. Eda, ACS Nano **7**, 791 (2013).
39) H. G. Ji, P. Solís-Fernández, U. Erkılıç, and H. Ago, ACS Appl. Nano Mater. **4**, 3717 (2021).